Geophysical Research Letters

RESEARCH LETTER
10.1029/2024GL112277

A Laboratory-Validated, Graph-Based Flow and Transport Model for Naturally Fractured Media

Collin R. Sutton[1] and **Christopher Zahasky**[1]

[1]Department of Geoscience, University of Wisconsin-Madison, Madison, WI, USA

Key Points:

- In situ and effluent experimental measurements of a conservative solute are used to quantify transport in a fractured core
- Tracer transport can be accurately modeled in fractured granite cores using graph-based modeling approaches
- The first high-resolution validation of a reduced physics model in fractured rock is presented

Supporting Information:

Supporting Information may be found in the online version of this article.

Correspondence to:

C. R. Sutton,
Collin.Sutton@wisc.edu

Citation:

Sutton, C. R., & Zahasky, C. (2024). A laboratory-validated, graph-based flow and transport model for naturally fractured media. *Geophysical Research Letters*, *51*, e2024GL112277. https://doi.org/10.1029/2024GL112277

Received 29 AUG 2024
Accepted 23 NOV 2024

© 2024. The Author(s).
This is an open access article under the terms of the Creative Commons Attribution License, which permits use, distribution and reproduction in any medium, provided the original work is properly cited.

Abstract Fractures are a primary feature controlling flow, transport, and coupled processes in geologic systems. To date, experimental image-based observations of these processes have been challenging. Here, we use pulse-tracer experiments with a conservative radiotracer ([^{18}F]-fludeoxyglucose) spanning multiple flow rates with simultaneous positron emission tomography imaging to characterize transport in a 5.08 cm fractured Sierra granite core. A graph-based, laboratory-validated flow and transport model is successfully demonstrated to describe the conservative solute transport in the natural fracture. Model network complexity, determined by the number of nodes and edges, significantly impacts model fit to observed data. Large graphs over-describe a fracture plane and act similarly to a porous medium while small graphs oversimplify the solute transport behavior. To our knowledge, this work provides the first validation of graph-based flow and transport models across a range of experimental conditions and sets the groundwork for upscaling to more complex and computationally efficient fracture models.

Plain Language Summary Fractures in rocks are important pathways for the movement of fluids and contaminants in the subsurface. While fractures in the subsurface are common, it is difficult to understand the contribution to fluid flow because fractures occupy a relatively small proportion of rock volume in the subsurface. In this study, we use a medical imaging technique called positron emission tomography to measure how fluids move through a fractured granite rock core. A new type of mathematical model is used to quantify and generalize how fluids move through fractured rock. The study found that the accuracy of the model depends on its complexity. If the model is too complex, it treats the fracture like a homogeneous porous material rather than a simple fracture. If it's too simple, it doesn't accurately represent fluid movement. This research validates these models against experimental measurements and lays the foundation for developing more advanced and efficient models for describing the flow of fluids and contaminants in fractures in the future.

1. Introduction

Understanding how to generalize single fracture variability while efficiently modeling fracture flow and transport remains a key gap in effectively describing flow and transport in fractured media. Field-scale fracture models rely on accurate representation of fracture connectivity and geometric features (e.g., aperture and size) (Karra et al., 2015). These features are directly related to the flow and transport where areas of high connectivity and larger aperture contribute to more flow. Field-based methods for describing fracture connectivity and geometry typically rely on outcrop mapping (Antonellini et al., 2017), borehole geophysical methods, photogrammetry (e.g., remote sensing or satellite-imagery) (Gili et al., 2022; Ma et al., 2023; Westoby et al., 2012), hydraulic testing (Illman, 2014; Guiltinan & Becker, 2015; Sayler et al., 2017; J. Patterson & Cardiff, 2023), or acoustic sensing (Becker et al., 2017; Johannessen et al., 2012). However, current field-based methods lack the necessary resolution to constrain the geometry of fracture systems, to characterize fracture flow based on physical properties such as aperture size and connectivity, and to quantify large differences between matrix and fracture flow properties (Illman, 2014; J. R. Patterson & Cardiff, 2023).

Single fractures have been extensively studied at the laboratory scale because they are considered the fundamental unit of flow and transport in a larger network of fractures (Viswanathan et al., 2022). Laboratory studies of single fracture systems enable the isolation of specific system parameters to construct process-based computational simulations which are important for upscaling lab-scale observations to the field scale (Viswanathan et al., 2022). Flow and transport is often inferred from defining the fracture geometry through ex-situ surface characterization or in situ imaging techniques (Ameli et al., 2013; Candela et al., 2009; Crandall et al., 2017; Dijk & Berkowitz, 1999; Kurotori et al., 2023; Wilson et al., 2011; Zahasky et al., 2019). Analog systems using transparent, 3D

UNCORRECTED PROOF

printed, or microfluidics experiments are also commonly used to explicitly measure flow and transport in fracture-like systems; however, these synthetic systems are often simplifications of natural systems due to material, dimensional, or spatial scale limitations (Isakov et al., 2001; Jiménez-Martínez et al., 2020; Kang et al., 2014; Lee & Kang, 2020; Morais et al., 2020; Radilla et al., 2013; Suzuki et al., 2017).

Experimental techniques that simulate natural fracture systems coupled with laboratory-validated modeling approaches are essential for advancing our understanding of fractured systems (Kang, Le Borgne et al., 2015; Kang et al., 2019; Viswanathan et al., 2022). In situ rock imaging techniques such as positron emission tomography (PET) offer an alternative approach to developing and validating models from experimental data by spatially and temporally quantifying high-resolution fluid channelization in fractured rock at the core-scale (Zahasky et al., 2019). PET has primarily been used to describe fluid flow and transport properties in fractured and porous media—specifically solute transport, multiphase flow, reactive transport, and colloid transport (Fernø et al., 2003; Kulenkampff et al., 2018; Kurotori et al., 2019; Le et al., 2023; Pingel et al., 2023; Pini et al., 2016; Sutton & Zahasky, 2024b; Zahasky & Benson, 2022; Zahasky et al., 2019).

In addition to challenges with flow and transport characterization, the spatially localized nature of fractures and their disproportional impact on subsurface flow and transport often require specialized modeling approaches. One of the most common modeling approaches for modeling flow and transport in fracture systems is discrete fracture network models (DFNs). DFNs explicitly define individual 2D or 3D fracture geometries that are meshed to solve for flow and transport with continuum methods based on assigned hydrological parameters (e.g., fracture aperture, permeability, and/or transmissivity). These networks can be created based on geological site characterization; however, stochastic approaches are typically employed to account for system uncertainty by generating many realizations that equally represent statistical fracture network data such as fracture density, spatial extent, and fracture orientations (Hyman et al., 2017). Despite advances in numerical techniques and high-performance computing, the computational demands of DFNs limit the number of model realizations and the ability to incorporate coupled processes such as geomechanics and reactive transport (Berrone et al., 2013, 2015; Hyman et al., 2015; Pichot et al., 2012).

Graph-based models have been recently used as a computationally efficient reduced-order approach to represent flow and transport in fracture networks (Hyman et al., 2017; Karra et al., 2015, 2018; Srinivasan et al., 2020; Viswanathan et al., 2018). Graph theory is the mathematical concept where a system can be defined as a set of nodes and edges or $G = (N, E)$, where G is the graph, N are nodes, and E are edges. Edges can be characterized by weights that represent some natural phenomena (Karra et al., 2018; Newman, 2004). This mathematical concept can be applied to fluid flow in fracture networks since flow is controlled by channels of different sizes (edges) and interconnections (nodes). Graphs are a more general form of the commonly-used lattice network approach to describe flow and transport processes in porous media (Oliveira et al., 2021; Rhodes & Blunt, 2006; Rhodes et al., 2008; Tsang et al., 1988). Graph-based modeling successfully describes flow and transport (de Dreuzy et al., 2012; Doolaeghe et al., 2020; Srinivasan, Hyman, Karra, O'Malley et al., 2018; Srinivasan, Hyman, Karra, Srinivasan, & Viswanathan, 2018; Srinivasan et al., 2020; Yang et al., 1995) and reduces the computational time of DFN modeling by up to three to four orders of magnitude (Karra et al., 2018; Viswanathan et al., 2018). A drawback to existing implementation methods is that graphs are created by extraction from a stochastically defined DFN (Hyman et al., 2017, 2018; Srinivasan et al., 2019; Valera et al., 2018; Viswanathan et al., 2022). Despite advances, graph-based modeling has yet to be validated against experiments or field observations at any scale. This study provides a standalone fracture modeling approach that is validated at the laboratory scale with implications for larger-scale studies.

2. Materials and Methods

Sierra granite blocks were fractured using a flexural bending test to create a naturally rough tensile fracture and then cored to retrieve 5.08 cm fractured cores. Matrix porosity was measured at 1.13% and permeability has been previously reported to be 10^{-18} m^2 (Moore & Glaser, 2007), thus matrix flow and transport was assumed to be negligible.

2.1. Experimental Methodology

Steady-state flow-through experiments with radiotracer injections in the naturally fractured 5.08 cm Sierra granite core were conducted using a specialized fluid injection system to collect image-based experimental solute

UNCORRECTED PROOF

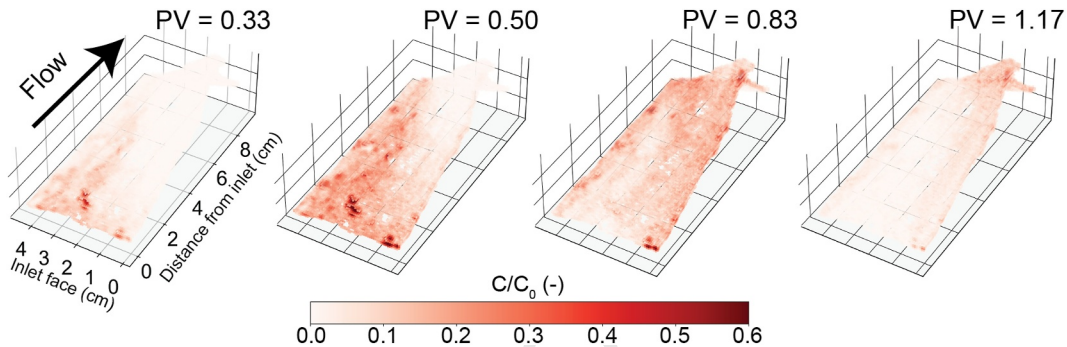


Figure 1. Segmented fracture plane plots from a 5.08 cm fractured granite core during flow-through injection of a 1 mL pulse of [^{18}F]-FDG injected at 0.5 mL/min from top to bottom at varying pore volumes injected (PV). The color scale shows voxel concentration normalized by the initial pulse concentration of radiotracer. Images are reconstructions of radiotracer location over a 60-s timestep. Voxel resolution is 0.07 × 0.07 × 0.08 cm. The signal-to-noise ratio for this experiment was calculated to be 507 based on the ratio of maximum voxel activity relative to the background activity in the image. This high signal-to-noise ratio is especially useful for identification and quantification of radiotracer concentrations in small features such as fractures. More qualitatively, these in situ images of radiotracer also highlight flow channelization and low-flow zones throughout the fractured granite core.

transport observations. The experimental workflow was to saturate the core under confining pressure with water until the differential pressure was stable.

After achieving fully saturated conditions, flow-through experiments were conducted at steady-state flow conditions with a discrete pulse of radiotracer imaged with PET. PET experiments were conducted at the University of Wisconsin Small Animal Imaging and Radiotherapy Facility using a (*Siemens Inveon DPET*) scanner with a 12 cm axial field of view. Fludeoxyglucose ([^{18}F]-FDG) was used as the radioisotope for PET imaging because it is commercially available and acts as a conservative tracer (Zahasky & Benson, 2018; Zahasky et al., 2019). A rotary valve and precisely measured lengths of tubing were used for pulse injections to enable continuous steady-state flow during tracer introduction, minimize dead volume, minimize pore pressure perturbations during tracer introduction, and ensure experiment repeatability and consistency. Injection pulse and effluent radiotracer concentrations were continuously measured with scintillation radiation sensors and the PET scan was concluded after all radiotracer had exited the core. These core-average breakthrough curves measured at the outlet of the experiment were used to validate model results. The exact experimental design is described in depth elsewhere (Sutton & Zahasky, 2024b). Additional background and methodological limits of PET for use in water resources can be found in Zahasky et al. (2019), and specific applications and quantification limits in fractures were recently reported in Kurotori et al. (2023).

A total of four experiments were conducted where the flow rate was controlled at either 0.5 mL/min or 1 mL/min and the pulse volume of radiotracer was 1 mL or 200 μL. Figure 1 shows PET images of solute transport at different pore volumes for the 0.5 mL/min with a 1 mL pulse injection experiment.

2.2. Graph Network Generation From Experimental Data

Graph geometry is constructed based on direct flow and transport observations from the PET data which affords the authors the chance to model a fracture directly rather than stochastically. Since direct observations of in situ flow and transport are highly unlikely in natural systems, a method was developed that could be applied to geologic data for network construction. Fracture network geometry is determined based on clustering as an approach that could be useful when a priori network geometry is unknown but geological properties, satellite imagery, or seismic data is available (Awad et al., 2018; Prabhakaran et al., 2021; Seifollahi et al., 2014). First, the maximum radiotracer concentration is calculated for each voxel to determine areas in the fracture with the largest fluxes. Second, the HDBSCAN clustering algorithm is used to identify clusters based on spatial relationships (Campello et al., 2013; Pedregosa et al., 2011).

Voxels below the 20th percentile corresponded with the imaging noise threshold and were ignored for graph construction. Lastly, the centroids of each cluster are used as the location of nodes and are connected (edges) by using the four nearest neighbors. The mean cluster concentration is used as the node concentration. Aperture size

UNCORRECTED PROOF

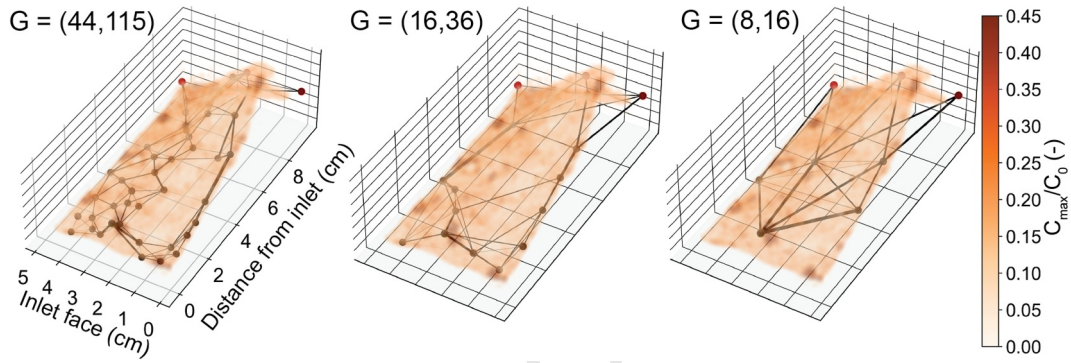


Figure 2. Graph networks (dots and lines) overlain on PET image of normalized voxel maximum concentration thresholded to exclude voxels with a local maximum concentration less than 20% of the total maximum concentration. Three red dots at the top of the plots represent outlet nodes and the inlet node is located near the inlet face center. This plot shows how graph construction changes the network representation of the fracture.

(b) is then related to the node concentration ($C_{\max}$) by $b_i = C_{\max_i} h/\alpha$. Here i is the node, h is the height of a voxel (0.078 cm) and α is a dimensionless scaling factor (0.7). The scaling factor is determined by fitting the modeled pressure drop to the pressure drop measured across the core during the experiments. The clustering approach can then be altered to produce many graphs of varying cluster density to determine model sensitivity to network geometry as illustrated in Figure 2. We created three geometries based on changing the HDBSCAN minimum cluster size parameter (i.e., 10, 15, 17 for most complex to simplest graph) to test our hypothesis that fluid channelization and transport in a single fracture plane would be oversimplified at some threshold once the network became too small. Currently, most fracture network models that use graphs or similar reduced-order approaches assume one fracture plane as a single edge or node. While no effort was made to optimize the graph size or node complexity, this is an area of future research that requires additional data sets to assess the generalizability of different clustering methods.

2.3. Numerical Flow and Transport Modeling Approach

The modeling approach consists of a flow solver and a transport solver. The flow solver calculates the pressure at each node (Moreno et al., 1988; Virtanen et al., 2020). The transport solver solves for individual particle transitions for a passive solute and accounts for particle advection, dispersion, and diffusion using a random-walk, particle tracking approach (Delay et al., 2005). Particle injection rules (e.g., uniform or flux-weighted) have been shown to have a significant impact on particle tracking statistics (Kang et al., 2017). We avoid these by injecting 10^5 particles at the inlet boundary node with an injection rule based on an experimentally measured injection pulse concentration binned at one-second intervals. Particles are assumed to follow a straight line path and streamline routing is assumed at each node (Berkowitz & Scher, 1997; Kang, Dentz, et al., 2015; Park et al., 2001). Streamline routing refers to moving a particle through an intersection on a direct route without any mass exchange with any other channel. Each particle transitions independently of other particles making this intrinsically parallelizable. The steps in the algorithm are listed below:

1. Create a graph with fracture geometry determined from PET data.
2. Solve the flow and pressure field where volumetric fluid flow is calculated based on Darcy's law using a constant flux at the inlet and a constant pressure head boundary at the outlet and assuming a laminar, viscous incompressible fluid through parallel plates (Moreno et al., 1988).
3. Calculate local velocities and Peclet numbers between connected nodes (Dentz et al., 2004; Oliveira et al., 2021).
4. Calculate probability of transitions between nodes $(p_{i,j})$ (Rhodes & Blunt, 2006; Rhodes et al., 2008), where node i is the current location of the particle.
5. Introduce particles at the inlet node(s) by sampling injection times (s) from a PDF that is calculated from the experimentally measured solute injection pulses.
6. Sample displacement direction $(p_{i,j})$ calculated in step 4 from the current node to the next node by generating a random number obtained from a normal distribution.

UNCORRECTED PROOF

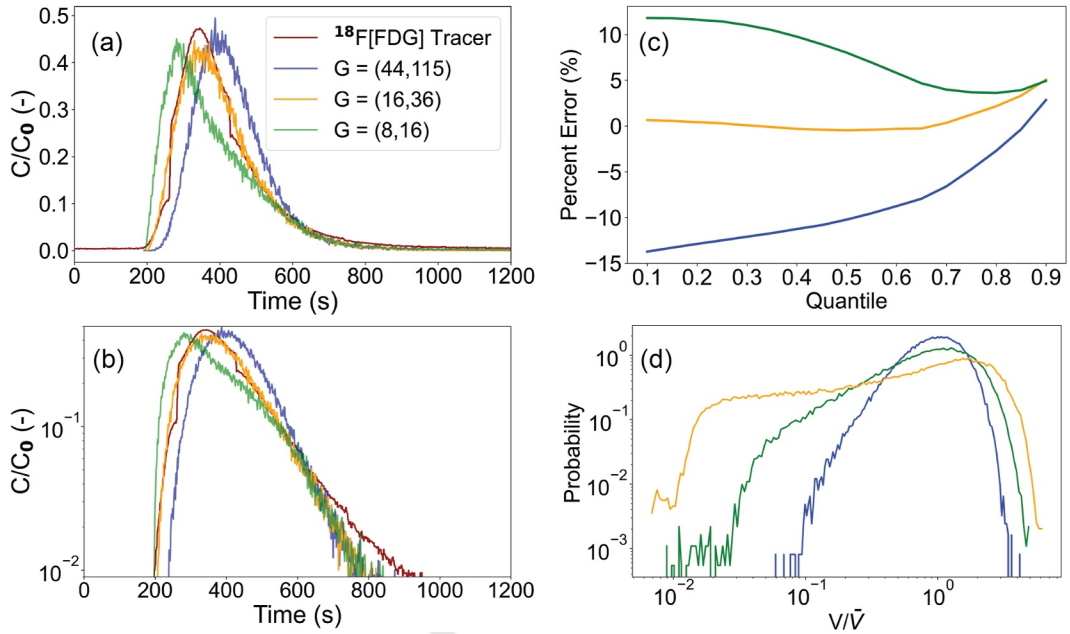


Figure 3. (a) Breakthrough curves of experimental (red) and transport models on a linear scale. Graphs from most (blue) to least (green) complex are shown. Model runtimes on an 11th Gen Intel i5-1135G7 are 29.5, 20.1, and 15.4 s respectively. (b) Breakthrough curves of experimental (red) and transport models on a log scale. (c) Percent error for each transport model is shown for each quantile calculated. (d) Lagrangian velocity distributions of the three different graphs are shown on a log concentration scale. These plots compare graph models to experimental data and show that graph complexity is a major factor in model fit.

7. Move the particle from node i to node j using the sampled displacement direction $(p_{i,j})$ and the calculated random-walk transit time $(T_{i,j})$ (Delay et al., 2005) and track particle location at discrete time steps.
8. Record breakthrough time for particle if it reaches an outlet or track until the simulation exceeds the experimental time.
9. Repeat steps 5–8 until each particle has a breakthrough or exceeds the experimental time.
10. A probability density function (PDF) of the particle arrival times, or breakthrough curve, is calculated and converted to concentration units by using the initial concentration of radiotracer injected and assigning a mass or radioactivity per particle injected such that the total mass of particles is equal to the total mass of solute injected.

A complete mathematical description of the steps in the algorithm can be found in the Supporting Information S1.

3. Results and Discussion

3.1. Effect of Graph Network Complexity

Graph network complexity, or the number of nodes and edges, significantly impacts breakthrough curve behavior of the model output. The effect of graph networks of different complexity is demonstrated by comparing the model breakthrough curves plotted in Figure 3 with the 0.5 mL/min injection and 1 mL tracer pulse experiment. The most complex graph, $G = (44, 115)$, has late breakthrough compared to experimental data and shows more Gaussian behavior. The graph $G = (16, 36)$ was found to closely match the breakthrough timing and shape of the experimental data with slight differences in the peak and the late stages of tailing behavior. The least complex graph, $G = (8, 16)$, shows similar breakthrough timing as the experimental data; however, it has a much steeper curve and significantly more tailing. The implication is that graphs can represent the physics of fracture flow and transport. However, too much complexity can lead to homogenization and a resemblance to a homogeneous porous media. Too little complexity leads to behavior that does not capture the dominant flow channels within the fracture.

UNCORRECTED

The network generation assumptions used in this study likely lead to a smoothing of the aperture field and, therefore, a homogenization of the velocity field leading to the observed Gaussian behavior of the most complex graph. It is assumed that if direct observations of the aperture field were used, then this effect would be negligible. The smoothing effect might be overcome in upscaling by using apertures sampled from probability distribution functions of the desired rock and fracture type which could mean that over-defining the network would only pose a computational limitation rather than a transport limitation. Additionally, flow paths have been shown to decrease to preferential routes as the scale increases and flow avoids unfavorable apertures and geometries, further enforcing the idea of over-defining the geometry (Pingel et al., 2023).

3.2. Breakthrough Curve Statistical Analysis

Breakthrough curve quantile analysis is used to quantitatively compare the transport model results with the experimental data (Harvey & Gorelick, 1995). Quantile analysis was performed every 5th quantile from the 10th to the 90th quantile. Values below the detection limit of the scintillation radiation sensors (0.009 mCi/mL) were omitted from the quantile analysis. Results are presented as percent error versus quantile where a positive error is an earlier arrival and a negative error is a later arrival compared to the experimentally-measured quantile. Comparisons between the three models and the experimental data are illustrated in Figure 3 and corroborate the behavior seen in the breakthrough curves. Graph $G = (44, 115)$ was consistently later than the experimental data while graph $G = (8, 16)$ exhibited significantly earlier arrival than the experimental data. Graph $G = (16, 36)$ closely matched experimental data until it deviated to an earlier arrival at late time. Statistical quantile analysis highlights that graph $G = (16, 36)$ is able to very closely fit the experimental breakthrough curve data.

Fractured rock modeling approaches that use graph models representing a fracture plane or fracture intersections as one edge typically have problems with initial breakthrough or late times (Hyman et al., 2017; Karra et al., 2018). Observations in this study indicate that representing a fracture plane as a single graph edge leads to an oversimplification of fluid channelization within the fracture. Simplified graph complexity leads to a lack of anomalous transport due to a reduction in diverse flow pathways. Lagrangian velocity statistics are used to quantify anomalous transport in the models arising from graph geometry. Lagrangian velocity statistics are the average particle, or group of particles, velocity along individual particle paths from inlet to outlet. This differs from an Eulerian perspective which uses a point in space as the observation point. Lagrangian approaches are more commonly used when anomalous transport occurs because they show dispersion and other transport processes (Kang, Dentz, et al., 2015; Le Borgne et al., 2008).

Velocity PDFs are shown in Figure 3d. We determine Lagrangian velocity PDFs by calculating volume-weighted histograms for each graph (Figure 2) and distance-averaging particle trajectories along each path (Perez et al., 2022). The most complex graph, $G = (44, 115)$, has the most condensed velocity distribution and approaches the expected behavior of a homogeneous porous medium. The least complex graph has a more elongated velocity distribution; however, the lowest velocities are mostly missed. The lack of graph complexity leads to more correlated flow channels and fast breakthrough with less realistic tailing behavior. The best fitting graph, $G = (16, 36)$, samples the widest range of velocities, and almost evenly samples velocities over three orders of magnitude. An intermediate amount of graph complexity allows for both correlation of fracture channels and velocity distribution due to trapping zones that more realistically simulate transport behavior in a realistic fracture.

Observations that velocity distributions with flat plateaus spanning orders of magnitude best describe fracture transport agree with previous, stochastically generated fracture network studies (Kang, Le Borgne et al., 2015; Kang et al., 2019). Velocity distribution and velocity correlation are key factors in modeling the transport behavior of tracers (Kang, Le Borgne et al., 2015). Early breakthrough is attributed to correlated velocities amongst large channels transporting particles more quickly from the inlet to the outlet (Kang et al., 2019). Late time tailing is attributed to broadening velocity distributions toward low-velocity values representing slow flow or trapping zones (Kang et al., 2019). Although not explored in the context of this study, velocity distribution and velocity correlation can be estimated from convergent and push-pull tracer tests, a promising avenue for graph-based modeling of cores without the assistance of PET data sets or in field settings.

UNCORRECTED PROOF

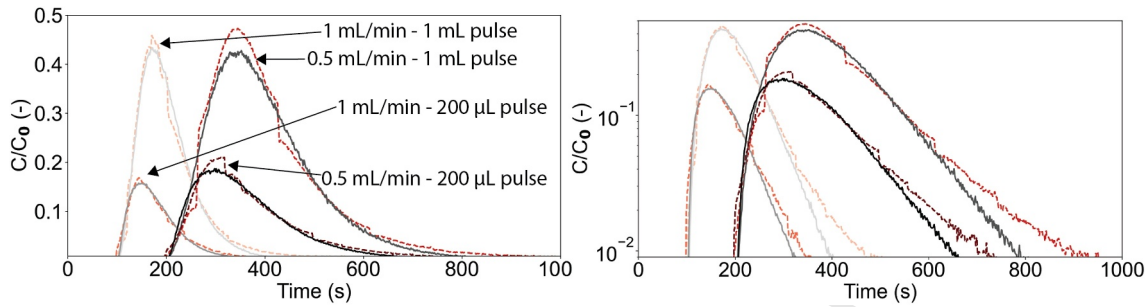


Figure 4. Breakthrough curves of the flow-through experiments (red) and the modeled predictions (grays). The left plot shows the experiments and models on a linear concentration scale and the right plot shows the data on a log concentration scale. This figure highlights the ability of a single reduced-physics graph model to accurately model four different experimental transport conditions in a fractured core.

3.3. Can the Model Be Predictive?

When applied to the other experiments, the best-fitting graph $G = (16, 36)$ predicts breakthrough behavior across a range of experimental conditions tested. Models with different flow and transport conditions (e.g., flow rate and pulse size) are validated against experimental data without changing graph geometry parameters or model transport parameters such as dispersivity. The only variables that were changed corresponded with changes in experimental conditions, specifically the flow rate and tracer pulse volume. Figure 4 shows the model results compared with the four different flow-through experiments. Results are remarkably similar to the breakthrough behavior in the experimental data. The timing of breakthrough and peak concentration match very well with some disagreement in all models at late time. This indicates that fracture geometry can be significantly simplified while closely describing the experimentally observed transport behavior.

Mismatch in the late time of the breakthrough curves is likely due to a combination of experimental and modeling factors. Experimentally, dead volume was minimized but not eliminated in the core holder end caps. This experimental artifact could result in the subtle diffusion-limited tailing behavior. Additionally, long tubing lengths from the inlet scintillation detector to the effluent scintillation detector are required for the core to be in the bore of the PET scanner which leads to excess Taylor dispersion and additional non-ideality in the inlet boundary conditions. In the model, graph geometry is the primary driver of particle dispersion due to fast channels and slow-flow zones while random walk only adds forward and backward dispersion. This is shown by the homogenization of breakthrough in very complex graphs and the fast breakthrough and poor matching of simple graphs. More complex numerical transport modeling methods such as multirate mass transfer or continuous time random walk have been shown to represent multidimensional particle trajectories (Kang, Dentz, et al., 2015; Kang et al., 2011, 2019). Additional transport complexity that could capture the subtle late-time tailing could be achieved by integrating these approaches into the particle transport modeling framework.

4. Conclusions

This letter presents a high-resolution, graph-based fracture model developed and validated on measured data. We show that single fracture conservative tracer transport behavior can be modeled and predicted with few degrees of freedom in a simple geometry. This work sets the foundation for determining large-scale fracture geometries by showing that fractures can be modeled without high-resolution meshing approaches. This is a key breakthrough for developing computationally efficient, multiscale fracture network models capable of predicting complex transport behavior in fractured systems. Future research aims to implement colloid transport, reactive solute transport, and fracture-matrix interactions to apply these methods across a wider range of applications and settings. This work also provides a foundation for future upscaling approaches for the application of graphs to field-scale fracture networks where geologic data can be clustered to form fracture network geometries (e.g., microseismic or acoustic emission data sets). This modeling method demonstrated on experimental data has broad implications across many fields and applications including fate and transport predictions of contamination hosted in fractured bedrock aquifers, modeling of heat transport in enhanced geothermal systems, fluid flow in fractured unconventional formations, and glacial fracture network hydrology.

UNCORRECTED PROOF

Data Availability Statement

Positron emission tomography (PET) data, laboratory data, and Python 3.0 were used in the creation of this manuscript. All scripts and supporting data are permanently available on HydroShare (Sutton & Zahasky, 2024a).

Acknowledgments
The authors thank Charlotte Bate, Hiroke Sone, and Maciej Trzeciak in the UW Madison Rock Mechanics Group for help and discussions developing the rock fracturing technique, coring, and obtaining porosity measurements. The experimental system used for coreflooding and imaging experiments was supported by the National Science Foundation under Grant 2002412. This work was supported by the Office of the Vice Chancellor for Research and Graduate Education at the University of Wisconsin-Madison with funding from the Wisconsin Alumni Research Foundation. Acknowledgment is made to the donors of the American Chemical Society Petroleum Research Fund for partial support of this research under project number 66040-DNI9.

References

Ameli, P., Elkhoury, J. E., & Detwiler, R. L. (2013). High-resolution fracture aperture mapping using optical profilometry. *Water Resources Research*, *49*(10), 7126–7132. https://doi.org/10.1002/wrcr.20501

Antonellini, M., Mollema, P. N., & Del Sole, L. (2017). Application of analytical diffusion models to outcrop observations: Implications for mass transport by fluid flow through fractures. *Water Resources Research*, *53*(7), 5545–5566. https://doi.org/10.1002/2016WR019864

Awad, M. A., Hassan, A. E., & Bekhit, H. M. (2018). The use of connectivity clusters in stochastic modelling of highly heterogeneous porous media. *Arabian Journal of Geosciences*, *11*(5), 98. https://doi.org/10.1007/s12517-018-3432-7

Becker, M. W., Ciervo, C., Cole, M., Coleman, T., & Mondanos, M. (2017). Fracture hydromechanical response measured by fiber optic distributed acoustic sensing at millihertz frequencies. *Geophysical Research Letters*, *44*(14), 7295–7302. https://doi.org/10.1002/2017GL073931

Berkowitz, B., & Scher, H. (1997). Anomalous transport in random fracture networks. *Physical Review Letters*, *79*(20), 4038–4041. https://doi.org/10.1103/PhysRevLett.79.4038

Berrone, S., Pieraccini, S., & Scialò, S. (2013). A PDE-constrained optimization formulation for discrete fracture network flows. *SIAM Journal on Scientific Computing*, *35*(2), B487–B510. https://doi.org/10.1137/120865884

Berrone, S., Pieraccini, S., Scialò, S., & Vicini, F. (2015). A parallel solver for large scale DFN flow simulations. *SIAM Journal on Scientific Computing*, *37*(3), C285–C306. https://doi.org/10.1137/140984014

Campello, R. J. G. B., Moulavi, D., & Sander, J. (2013). Density-based clustering based on hierarchical density estimates. In J. Pei, V. S. Tseng, L. Cao, H. Motoda, & G. Xu (Eds.), *Advances in knowledge discovery and data mining* (pp. 160–172). Springer Berlin Heidelberg.

Candela, T., Renard, F., Bouchon, M., Brouste, A., Marsan, D., Schmittbuhl, J., & Voisin, C. (2009). Characterization of fault roughness at various scales: Implications of three-dimensional high resolution topography measurements. *Pure and Applied Geophysics*, *166*(10), 1817–1851. https://doi.org/10.1007/s00024-009-0521-2

Crandall, D., Moore, J., Gill, M., & Stadelman, M. (2017). CT scanning and flow measurements of shale fractures after multiple shearing events. *International Journal of Rock Mechanics and Mining Sciences*, *100*, 177–187. https://doi.org/10.1016/j.ijrmms.2017.10.016

de Dreuzy, J.-R., Méheust, Y., & Pichot, G. (2012). Influence of fracture scale heterogeneity on the flow properties of three-dimensional discrete fracture networks (DFN). *Journal of Geophysical Research*, *117*(B11), B11207. https://doi.org/10.1029/2012JB009461

Delay, F., Ackerer, P., & Danquigny, C. (2005). Simulating solute transport in porous or fractured formations using random walk particle tracking: A review. *Vadose Zone Journal*, *4*(2), 360–379. https://doi.org/10.2136/vzj2004.0125

Dentz, M., Cortis, A., Scher, H., & Berkowitz, B. (2004). Time behavior of solute transport in heterogeneous media: Transition from anomalous to normal transport. *Advances in Water Resources*, *27*(2), 155–173. https://doi.org/10.1016/j.advwatres.2003.11.002

Dijk, P. E., & Berkowitz, B. (1999). Three-dimensional flow measurements in rock fractures. *Water Resources Research*, *35*(12), 3955–3959. https://doi.org/10.1029/1999WR900200

Doolaeghe, D., Davy, P., Hyman, J. D., & Darcel, C. (2020). Graph-based flow modeling approach adapted to multiscale discrete-fracture-network models. *Physical Review E - Statistical Physics, Plasmas, Fluids, and Related Interdisciplinary Topics*, *102*(5–1), 053312. https://doi.org/10.1103/physreve.102.053312

Fernø, M. A., Hauge, L. P., Rognmo, A. U., Gauteplass, J., & Graue, A. (2003). Flow visualization of CO_2 in tight shale formations at reservoir conditions. *Geophysical Research Letters*, 7414–7419. https://doi.org/10.1002/2015GL065100.Received

Gili, J. A., Ruiz-Carulla, R., Matas, G., Moya, J., Prades, A., Corominas, J., et al. (2022). Rockfalls: Analysis of the block fragmentation through field experiments. *Landslides*, *19*(5), 1009–1029. https://doi.org/10.1007/s10346-021-01837-9

Guiltinan, E., & Becker, M. W. (2015). Measuring well hydraulic connectivity in fractured bedrock using periodic slug tests. *Journal of Hydrology*, *521*, 100–107. https://doi.org/10.1016/j.jhydrol.2014.11.066

Harvey, C. F., & Gorelick, S. M. (1995). Mapping hydraulic conductivity: Sequential conditioning with measurements of solute arrival time, hydraulic head, and local conductivity. *Water Resources Research*, *31*(7), 1615–1626. https://doi.org/10.1029/95WR00547

Hyman, J. D., Hagberg, A., Osthus, D., Srinivasan, S., Viswanathan, H., & Srinivasan, G. (2018). Identifying backbones in three-dimensional discrete fracture networks: A bipartite graph-based approach. *Multiscale Model Simulation*, *16*(4), 1948–1968. https://doi.org/10.1137/18m1180207

Hyman, J. D., Hagberg, A., Srinivasan, S., & Viswanathan, H. (2017). Predictions of first passage times in sparse discrete fracture networks using graph-based reductions. *Physical Review*, *96*, 1–10. 013304. https://doi.org/10.1103/PhysRevE.96.013304

Hyman, J. D., Karra, S., Makedonska, N., Gable, C. W., Painter, S. L., & Viswanathan, H. S. (2015). dfnWorks: A discrete fracture network framework for modeling subsurface flow and transport. *Computers & Geosciences*, *84*, 10–19. https://doi.org/10.1016/j.cageo.2015.08.001

Illman, W. A. (2014). Hydraulic tomography offers improved imaging of heterogeneity in fractured rocks. *Groundwater*, *52*(5), 659–684. https://doi.org/10.1111/gwat.12119

Isakov, E., Ogilvie, S. R., Taylor, C. W., & Glover, P. W. (2001). Fluid flow through rough fractures in rocks I: High resolution aperture determinations. *Earth and Planetary Science Letters*, *191*(3), 267–282. https://doi.org/10.1016/S0012-821X(01)00424-1

Jiménez-Martínez, J., Hyman, J. D., Chen, Y., Carey, J. W., Porter, M. L., Kang, Q., et al. (2020). Homogenization of dissolution and enhanced precipitation induced by bubbles in multiphase flow systems. *Geophysical Research Letters*, *47*(7), e2020GL087163. https://doi.org/10.1029/2020GL087163

Johannessen, K., Drakeley, B., & Farhadiroushan, M. (2012). Distributed acoustic sensing - a new way of listening to your well/reservoir (Vol. SPE-149602-MS). https://doi.org/10.2118/149602-MS

Kang, P. K., de Anna, P., Nunes, J. P., Bijeljic, B., Blunt, M. J., & Juanes, R. (2014). Pore-scale intermittent velocity structure underpinning anomalous transport through 3-D porous media. *Geophysical Research Letters*, *41*(17), 6184–6190. https://doi.org/10.1002/2014GL061475

Kang, P. K., Dentz, M., Le Borgne, T., & Juanes, R. (2011). Spatial Markov model of anomalous transport through random lattice networks. *Physical Review Letters*, *107*(18), 180602. https://doi.org/10.1103/PhysRevLett.107.180602

Kang, P. K., Dentz, M., Le Borgne, T., & Juanes, R. (2015). Anomalous transport on regular fracture networks: Impact of conductivity heterogeneity and mixing at fracture intersections. *Physical Review E - Statistical Physics, Plasmas, Fluids, and Related Interdisciplinary Topics*, *92*(2), 022148. https://doi.org/10.1103/PhysRevE.92.022148

UNCORRECTED PROOF

Kang, P. K., Dentz, M., Le Borgne, T., Lee, S., & Juanes, R. (2017). Anomalous transport in disordered fracture networks: Spatial Markov model for dispersion with variable injection modes. *Advances in Water Resources*, *106*, 80–94. (Tribute to Professor Garrison Sposito: An Exceptional Hydrologist and Geochemist). https://doi.org/10.1016/j.advwatres.2017.03.024

Kang, P. K., Le Borgne, T., Dentz, M., Bour, O., & Juanes, R. (2015). Impact of velocity correlation and distribution on transport in fractured media: Field evidence and theoretical model. *Water Resources Research*, *51*(2), 940–959. https://doi.org/10.1002/2014WR015799

Kang, P. K., Lei, Q., Dentz, M., & Juanes, R. (2019). Stress-induced anomalous transport in natural fracture networks. *Water Resources Research*, *55*(5), 4163–4185. https://doi.org/10.1029/2019WR024944

Karra, S., Makedonska, N., Viswanathan, H. S., Painter, S. L., & Hyman, J. D. (2015). Effect of advective flow in fractures and matrix diffusion on natural gas production. *Water Resources Research*, *51*(10), 8646–8657. https://doi.org/10.1002/2014WR016829

Karra, S., Malley, D. O., Hyman, J. D., Viswanathan, H. S., & Srinivasan, G. (2018). Modeling flow and transport in fracture networks using graphs. *Physical Review*, *97*(033304), 1–9. https://doi.org/10.1103/PhysRevE.97.033304

Kulenkampff, J., Sto, M., Gründig, M., Manse, A., Lippmann-pipke, J., & Kersten, M. (2018). Time-lapse 3D imaging by positron emission tomography of Cu mobilized in a soil column by the herbicide MCPA. *Scientific Reports*, 1–9. https://doi.org/10.1038/s41598-018-25413-9

Kurotori, T., Zahasky, C., Gran, M., Kovscek, A. R., & Benson, S. M. (2023). Comparative analysis of imaging and measurements of micrometer - Scale fracture aperture fields within a heterogeneous rock using PET and X - Ray CT. *Transport in Porous Media*, *147*(3), 519–539. https://doi.org/10.1007/s11242-023-01922-8

Kurotori, T., Zahasky, C., Hosseinzadeh Hejazi, S. A., Shah, S. M., Benson, S. M., & Pini, R. (2019). Measuring, imaging and modelling solute transport in a microporous limestone. *Chemical Engineering Science*, *196*, 366–383. https://doi.org/10.1016/j.ces.2018.11.001

Le, V., Thompson, S., Roden, E., & Zahasky, C. (2023). In situ measurements of dynamic bacteria transport and attachment in heterogeneous sand-packed columns. *Environmental Science & Technology*, *57*(41), 15588–15597. (PMID: 37782746). https://doi.org/10.1021/acs.est.3c02197

Le Borgne, T., Dentz, M., & Carrera, J. (2008). Spatial Markov processes for modeling Lagrangian particle dynamics in heterogeneous porous media. *Physical Review E - Statistical Physics, Plasmas, Fluids, and Related Interdisciplinary Topics*, *78*(2), 026308. https://doi.org/10.1103/PhysRevE.78.026308

Lee, S. H., & Kang, P. K. (2020). Three-dimensional vortex-induced reaction hot spots at flow intersections. *Physical Review Letters*, *124*(14), 144501. https://doi.org/10.1103/PhysRevLett.124.144501

Ma, T., Zhang, D., Li, X., Huang, Y., Zhang, L., Zhu, Z., et al. (2023). Hyperspectral remote sensing technology for water quality monitoring: Knowledge graph analysis and Frontier trend. *Frontiers in Environmental Science*, *11*. https://doi.org/10.3389/fenvs.2023.1133325

Moore, J. R., & Glaser, S. D. (2007). Self-potential observations during hydraulic fracturing. *Journal of Geophysical Research*, *112*(B2), B02204. https://doi.org/10.1029/2006JB004373

Morais, S., Cario, A., Liu, N., Bernard, D., Lecoutre, C., Garrabos, Y., et al. (2020). Studying key processes related to CO2 underground storage at the pore scale using high pressure micromodels. *Reaction Chemistry & Engineering*, *5*(7), 1156–1185. https://doi.org/10.1039/D0RE00023J

Moreno, L., Tsang, Y. W., Tsang, C. F., Hale, F. V., & Neretnieks, I. (1988). Flow and tracer transport in a single fracture: A stochastic model and its relation to some field observations. *Water Resources Research*, *24*(12), 2033–2048. https://doi.org/10.1029/WR024i012p02033

Newman, M. E. J. (2004). Analysis of weighted networks. *Physical Review E - Statistical Physics, Plasmas, Fluids, and Related Interdisciplinary Topics*, *70*(5), 056131. https://doi.org/10.1103/PhysRevE.70.056131

Oliveira, R., Bijeljic, B., Blunt, M. J., Colbourne, A., Sederman, A. J., Mantle, M. D., & Gladden, L. F. (2021). A continuous time random walk method to predict dissolution in porous media based on validation of experimental NMR data. *Advances in Water Resources*, *149*, 103847. https://doi.org/10.1016/j.advwatres.2021.103847

Park, Y.-J., de Dreuzy, J.-R., Lee, K.-K., & Berkowitz, B. (2001). Transport and intersection mixing in random fracture networks with power law length distributions. *Water Resources Research*, *37*(10), 2493–2501. https://doi.org/10.1029/2000WR000131

Patterson, J., & Cardiff, M. (2023). Stiff, smooth, and solid? Complex fracture hydraulics' imprint on oscillatory hydraulic testing. *Water Resources Research*, *59*(11), e2023WR034621. https://doi.org/10.1029/2023WR034621

Patterson, J. R., & Cardiff, M. (2023). Do simple analytical models capture complex fractured bedrock hydraulics? Oscillatory flow tests suggest not. *Groundwater*, *61*(6), 816–833. https://doi.org/10.1111/gwat.13297

Pedregosa, F., Varoquaux, G., Gramfort, A., Michel, V., Thirion, B., Grisel, O., et al. (2011). Scikit-learn: Machine learning in Python. *Journal of Machine Learning Research*, *12*, 2825–2830. Retrieved from http://www.jmlr.org/papers/volume12/pedregosa11a/pedregosa11a.pdf

Perez, L. J., Parashar, R., Plymale, A., & Scheibe, T. D. (2022). Contributions of biofilm-induced flow heterogeneities to solute retention and anomalous transport features in porous media. *Water Research*, *209*, 117896. https://doi.org/10.1016/j.watres.2021.117896

Pichot, G., Erhel, J., & de Dreuzy, J.-R. (2012). A generalized mixed hybrid mortar method for solving flow in stochastic discrete fracture networks. *SIAM Journal on Scientific Computing*, *34*(1), B86–B105. https://doi.org/10.1137/100804383

Pingel, J. L., Kulenkampff, J., Jara-Heredia, D., Stoll, M., Zhou, W., Fischer, C., & Schäfer, T. (2023). In-situ flow visualization with geo-positron-emission-tomography in a granite fracture from Soultz-Sous-Forêts, France. *Geothermics*, *111*, 102705. https://doi.org/10.1016/j.geothermics.2023.102705

Pini, R., Vandehey, N. T., Druhan, J., Neil, J. P. O., & Benson, S. M. (2016). Quantifying solute spreading and mixing in reservoir rocks using 3-D PET imaging. *Journal of Fluid Mechanics*, *796*, 558–587. https://doi.org/10.1017/jfm.2016.262

Prabhakaran, R., Bertotti, G., Urai, J., & Smeulders, D. (2021). Investigating spatial heterogeneity within fracture networks using hierarchical clustering and graph distance metrics. *Solid Earth*, *12*(10), 2159–2209. https://doi.org/10.5194/se-12-2159-2021

Radilla, G., Nowamooz, A., & Fourar, M. (2013). Modeling non-Darcian single- and two-phase flow in transparent replicas of rough-walled rock fractures. *Transport in Porous Media*, *98*(2), 401–426. https://doi.org/10.1007/s11242-013-0150-1

Rhodes, M. E., Bijeljic, B., & Blunt, M. J. (2008). Pore-to-field simulation of single-phase transport using continuous time random walks. *Advances in Water Resources*, *31*(12), 1527–1539. https://doi.org/10.1016/j.advwatres.2008.04.006

Rhodes, M. E., & Blunt, M. J. (2006). An exact particle tracking algorithm for advective-dispersive transport in networks with complete mixing at nodes. *Water Resources Research*, *42*(4), W04501. https://doi.org/10.1029/2005WR004504

Sayler, C., Cardiff, M., & Fort, M. D. (2017). Understanding the geometry of connected fracture flow with multiperiod oscillatory hydraulic tests. *Ground Water*, *56*(2), 276–287. https://doi.org/10.1111/gwat.12580

Seifollahi, S., Dowd, P. A., Xu, C., & Fadakar, A. Y. (2014). A spatial clustering approach for stochastic fracture network modelling. *Rock Mechanics and Rock Engineering*, *47*(4), 1225–1235. https://doi.org/10.1007/s00603-013-0456-x

Srinivasan, S., Hyman, J., Karra, S., O'Malley, D., Viswanathan, H., & Srinivasan, G. (2018). Robust system size reduction of discrete fracture networks: A multi-fidelity method that preserves transport characteristics. *Computational Geosciences*, *22*(6), 1515–1526. https://doi.org/10.1007/s10596-018-9770-4

UNCORRECTED PROOF

Srinivasan, S., Hyman, J., Karra, S., Srinivasan, G., & Viswanathan, H. (2018). Reduced-order models of discrete fracture networks through flow-physics on graph representations (Vols. Day 3 Fri, June 22, 2018).

Srinivasan, S., Karra, S., Hyman, J., Viswanathan, H., & Srinivasan, G. (2019). Model reduction for fractured porous media: A machine learning approach for identifying main flow pathways. *Computational Geosciences*, *23*(3), 617–629. https://doi.org/10.1007/s10596-019-9811-7

Srinivasan, S., O'Sullivan, D., Hyman, J. D., Karra, S., Viswanathan, H. S., & Srinivasan, G. (2020). Transient flow modeling in fractured media using graphs. *Physical Review E*, *102*(5), 52310. https://doi.org/10.1103/PhysRevE.102.052310

Sutton, C., & Zahasky, C. (2024a). Graph-based flow and transport model and dataset for fractured granite core [Dataset]. *Hydroshare*. https://doi.org/10.4211/hs.0433d48779f94704b4e1b983f5e41da6

Sutton, C., & Zahasky, C. (2024b). In situ quantification of colloidal kaolinite transport and attachment in porous media using positron emission tomography. *Transport in Porous Media*, *151*(8), 1755–1775. https://doi.org/10.1007/s11242-024-02093-w

Suzuki, A., Watanabe, N., Li, K., & Horne, R. N. (2017). Fracture network created by 3-D printer and its validation using CT images. *Water Resources Research*, *53*(7), 6330–6339. https://doi.org/10.1002/2017WR021032

Tsang, Y. W., Tsang, C. F., Neretnieks, I., & Moreno, L. (1988). Flow and tracer transport in fractured media' a variable aperture channel model and its properties. *Water Resources Research*, *24*(12), 2049–2060. https://doi.org/10.1029/wr024i012p02049

Valera, M., Guo, Z., Kelly, P., Matz, S., Adrian, V., Percus, A. G., et al. (2018). Machine learning for graph-based representations of three-dimensional discrete fracture networks connected networks of fractures are the primary pathways. *Computational Geosciences*, *22*(3), 695–710. https://doi.org/10.1007/s10596-018-9720-1

Virtanen, P., Gommers, R., Oliphant, T. E., Haberland, M., Reddy, T., Cournapeau, D., et al., SciPy 1.0 Contributors. (2020). SciPy 1.0: Fundamental algorithms for scientific computing in Python. *Nature Methods*, *17*(3), 261–272. https://doi.org/10.1038/s41592-019-0686-2

Viswanathan, H. S., Ajo-Franklin, J., Birkholzer, J. T., Carey, J. W., Guglielmi, Y., Hyman, J. D., et al. (2022). From fluid flow to coupled processes in fractured rock: Recent advances and new frontiers. *Reviews of Geophysics*, *60*(1), 1–65. https://doi.org/10.1029/2021RG000744

Viswanathan, H. S., Hyman, J. D., Karra, S., O'Sullivan, D., Srinivasan, S., Hagberg, A., & Srinivasan, G. (2018). Advancing graph-based algorithms for predicting flow and transport in fractured rock. *Water Resources Research*, *54*(9), 6085–6099. https://doi.org/10.1029/2017WR022368

Westoby, M., Brasington, J., Glasser, N., Hambrey, M., & Reynolds, J. (2012). Structure-from-Motion' photogrammetry: A low-cost, effective tool for geoscience applications. *Geomorphology*, *179*, 300–314. https://doi.org/10.1016/j.geomorph.2012.08.021

Wilson, C. E., Aydin, A., Karimi-Fard, M., Durlofsky, L. J., Amir, S., Brodsky, E. E., et al. (2011). From outcrop to flow simulation: Constructing discrete fracture models from a LIDAR survey. *AAPG Bulletin*, *95*(11), 1883–1905. https://doi.org/10.1306/03241108148

Yang, G., Myer, L. R., Brown, S. R., & Cook, N. G. W. (1995). Microscopic analysis of macroscopic transport properties of single natural fractures using graph theory algorithms. *Geophysical Research Letters*, *22*(11), 1429–1432. https://doi.org/10.1029/95GL01498

Zahasky, C., & Benson, S. M. (2018). Micro-positron emission tomography for measuring sub-core scale single and multiphase transport parameters in porous media. *Advances in Water Resources*, *115*, 1–16. https://doi.org/10.1016/j.advwatres.2018.03.002

Zahasky, C., & Benson, S. M. (2022). Preferential solute transport in low permeability zones during spontaneous imbibition in heterogeneous porous media. *Water Resources Research*, *58*(1), e2020WR029460. https://doi.org/10.1029/2020wr029460

Zahasky, C., Kurotori, T., Pini, R., & Benson, S. M. (2019). Positron emission tomography in water resources and subsurface energy resources engineering research. *Advances in Water Resources*, *127*, 39–52. https://doi.org/10.1016/j.advwatres.2019.03.003

References From the Supporting Information

Bear, J. (1988). *Dynamics of fluids in porous media*. American Elsevier.

UNCORRECTED PROOF